

Measuring the Binding Constant for Gold Nanospheres to Synthetic Phospholipid Membranes

Gordon R. Watson

April 21st, 2022

Department of Chemistry and Biochemistry

Mount Allison University

Honours B.Sc. Biochemistry

Abstract

Effective use of nanoparticles in clinical applications requires a thorough understanding of their numerous interactions in biological environments. The interaction of nanoparticle adhesion to cellular environments has yet to be quantified, which may reveal the physical or biological mechanisms that drive nanoparticles to interact with cells. The binding affinity constant (K_b) is a value used for describing the toxicity of materials that may enter the body as well as the selectivity of drug designs. To this end, this study aims to develop a method that would effectively quantify the binding of spherical gold nanoparticles (AuNP) to a synthetic phospholipid monolayer either entirely composed of DPPC or POPG. models were compared in determining K_b : the Langmuir adsorption isotherm and Michaelis–Menten binding saturation kinetics. Both models determined K_b for AuNP interaction, with the Langmuir adsorption isotherm delivering a more precise and sensitive range. The determined K_b values for DPPC@AuNP and POPG@AuNP using the Langmuir adsorption isotherm was 213 ± 6 and 115 ± 8 respectfully. Our K_b values also indicated that charge interactions between the phospholipid head group and gold nanoparticle surface significantly affects the strength of nanoparticle adsorption ($P=0.0032$).

Acknowledgments

I would like to take this time to acknowledge and thank Dr. M. -Vicki Meli for her patience, guidance, and support throughout my research for my honors project. Her wisdom instilled confidence in me when it came to the scientific process and in moving forward in the next step of my academic career, and for that I am grateful.

I would also like to thank Dr. Tyson MacCormack for his support through my honors project and for being my second reader. His insight was invaluable.

Thank you, Steve Cogswell, for developing the TEM images of my gold nanoparticles.

The Nanomeli lab holds memories and experiences I will look back fondly on. While the pandemic limited the activities we could pursue together, every member in the lab made the experience much better, placing humanity in research, where while our goals may be different, we all embarked on the same journey of discovery together.

A special thanks to Kate Leslie for indulging my theoretical questions about Nanoscience, and overall, being an amazing lab partner.

Lastly, I would like to thank Mount Allison University for awarding me with the R. P. Chapman award to help fund my honors project.

Table of Contents

1. Introduction

- 1.1 What are nanoparticles and how are they used in medicine?.....pg. 6-7
- 1.2 Nanoparticle properties affect their biological fate.....pg. 7-9
- 1.3 Interactions at the lipid membrane environment determine nanoparticle internalization pg. 9-12
- 1.4 Aim of research..... pg. 12-13

2. Methods

- 2.1: Reagents and solutions..... pg. 14
- 2.2: Nanoparticle synthesis and characterization.....pg. 15-16
- 2.3: Membrane spreading and nanoparticle exposure..... pg. 16-17
- 2.5: Michalis-Menten binding kinetics and calculations.....pg. 17-18
- 2.6: Langmuir Adsorption Isotherm and Calculations.....pg. 18

3. Results

- 3.1: The binding affinity constants determined using Michaelis–Menten Binding Saturation Kinetics.....pg. 19-20
- 3.2: The binding affinity constants determined using Langmuir Adsorption Isotherm..... pg. 21-22

4. Discussion & Conclusion

- 4.1: Model and Experimental Evaluation.....pg. 23-24
- 4.2: K_b interpretation and biological relevance..... pg. 24-25
- 4.3: Future Directions pg. 25-26
- 4.4: Conclusion pg. 26

References.....pg. 27-30

Supplemental Data.....pg. 31

List of Figures

Figure 1: The interaction of nano-sized materials at the cellular surface and the nanoparticle properties that affect their cellular interactions

Figure 2: The chemical structure of DPPC and POPG

Figure 3: The comparison of binding saturation curves developed using Michaelis–Menten Binding Saturation Kinetics for AuNPs to the surfaces of DPPC and POPG monolayers

Figure 4: The comparison of linear regressions developed using the Langmuir Adsorption Isotherm for AuNPs to the surface of DPPC and POPG monolayers

Chapter 1

Introduction

1.1: What are Nanoparticles and how are they used in medicine?

Nanoparticles have been in recent interest within the medical field. How nanoparticles interact once in contact with a biological system is yet to be fully understood. Nanoparticles are materials whose sizes range from 1-100 nm in scale¹. Their physical and chemical properties give them huge potential in their engineering for drug delivery, imaging, and even treatment for cancer and other diseases². Nanoparticles can be functionalized by the core element, size, shape, charge, and the nature of the attached ligand. Altering these parameters can affect how nanoparticles distribute and target cells in the body^{3,4}.

Nanoparticles can be functionalized by a large variety of capping agents which can prevent their agglomeration in solution, affect the nanoparticle's size, adjust the nanoparticle's catalytic ability, and alter how they behave in the biological environment^{5,6}. Common capping agents includes thiols, polymers, or bulky, charged organic molecules such as citrate⁷. Capping agents can be terminated with anionic or cationic functional groups, fluorophores, or cytotoxic molecules, diversifying the roles nanoparticles can play². A common capping agent used today is polyethylene glycol (PEG). PEG is very soluble in water and biocompatible with many cells, making it a very useful capping agent for use in nanomedicine⁸. Once in a biological environment, such as human serum, metal nanoparticles often adsorb proteins, forming a biomolecular corona on its surface. Earlier, it was thought when functionalized with PEG, these nanoparticles may avoid adsorption of such proteins, however, recent studies indicate that the

supposed stealthing effect is conferred by specifically adsorbed corona proteins on the PEGylated surface of the nanoparticles⁹.

As research continued contributing further understanding of the chemical, physical and biological properties of nanoparticles, so did the endeavors rise from medical scientists to discerning their uses in improving the health of patients. For example in the use of nanoparticles in today's medicine: lipid nanoparticles (LNP) are used as drug transporters in gene therapy, quantum dots can be used as imaging agents for *in vivo* microscopy, and gold nanorods can be used in treating cancer tumors². Understanding the biological interactions and affinity of nanomaterials at the cellular level may we raise the floor of clinical research to new possibilities.

Currently, the nanomedicine field has made huge contributions to the battle against Covid-19. Pfizer and Moderna manufactured vaccines that utilized lipid nanoparticle shells which transport the mRNA effectively to the right location in cells for the vaccine. Both utilize functionalized PEG in their lipid caps¹⁰. However, utilizing PEG ligands as a capping agent is novel in the medicinal field and the effect that PEG can have in inducing anaphylaxis in some patients raises concern^{11,12}.

1.2: Nanoparticle properties affect their biological interactions

Nanomedicine is a wide and growing field that can treat a wide range of illnesses. In medicine, nanoparticles are commonly used as delivery vehicles to transport drugs to the targeted site². When talking about nanoparticles in the biological environment, it is good to keep in mind the common biomolecules that exist at the nanoscale. Proteins, DNA, and even viruses exist in the relative size of commonly synthesized nanoparticles between 1-100 nm in diameter.

Nanoparticles can thus interact with these molecules in dynamic ways be it through causing a temporary structural change in these biomolecules, or irreversibly adsorbing them¹³.

Nanoparticles can enter the biological system through inhalation, skin adsorption, or orally. Because of their size, nanoparticles can freely pass through common biological barriers and be easily moved through the circulation system, meaning they can target nearly any cell in the body¹⁴. There is strong evidence that nanoparticle size and coating both have a strong influence on the intracellular fate of nanoparticles. Nanoparticles less than 10 nm in size behave similarly to gasses in how they easily enter human tissue and disrupt the biochemical environment¹⁵. As a nanoparticle gets smaller, its surface area to volume ratio dramatically increases, meaning fewer atoms are buried in the core of the particle and can interact with their environment. As such, the magnitude of the toxic effect exerted by a nanoparticle is inversely proportional to the particle's size¹⁶.

With the increasing use of nanoparticles in consumer goods, such as clothing, sunscreens, and even preserved food, it is important to further understanding the harmful effects these objects might pose to human and animal life¹⁷. The mechanisms of toxicity for nanoparticles are far from being understood, specifically for the interactions between nanoparticles and biological molecules. As stated earlier, LNPs are largely innocuous and biocompatible, however, many metal nanoparticles have been screened for genotoxicity and cytotoxicity¹⁸. For example, silver nanoparticles, often used in athletic clothing and as anti-microbial reagents have displayed toxic effects in the liver, kidneys and lungs by disturbing cell membrane integrity and causing oxidative stress on cells through the formation of reactive oxygen species^{19,20}. Most metal nanoparticles also adsorb proteins in the biological system, which causes slight denaturation of

the protein and causing loss of function in that protein. This can sometimes impede cellular metabolism or function depending on which proteins are adsorbed⁹.

Regardless, metal nanoparticles can still be exploited to treat many illnesses. Gold nanoparticles (AuNP) are a prime example of metal nanoparticles that are used in medicine today. AuNPs are used as drug capsules which increase the efficiency and specificity of drug transport²¹. They can be easily functionalized through binding thiols with carboxylic or amine groups, adding to their diversity for utilization in medicine¹⁹. AuNPs are considered relatively safe, as the gold core is inert and not as toxic compared to silver and copper oxide²⁰. AuNP is often used in treating cancers as it can target and induce apoptotic cell death in many cancerous tissues. This is usually achieved through targeting the nanoparticles once at the tumor site with a laser that applies near-infrared light to the AuNP which is harmless to healthy human tissue and will cause the AuNP to produce localized heat and induces cell death in a targeted manner²².

A huge challenge for using nanoparticles to treat cancer is that up to 90 % of nanoparticles are lost due to undergoing extensive first-phase metabolism in the liver²³. Much research is still going into improving the targetability and minimizing the loss of nanoparticles once in the biological environment².

1.3: Interactions in the lipid membrane environment determine nanoparticle internalization

A major constituent of a cell is the phospholipid environment, known as the cell membrane, which surrounds and protects the cell's body, separating it from the external environment. Cellular membranes are largely composed of phospholipids, proteins, glycolipids, and sterols²⁴. This dynamic environment can be altered depending on the cells' function in the

body, thus, the cellular membrane can be a dynamic functional environment. Common structural and chemical changes that make one cell differ include the type of phospholipid that predominates its surface which differs by their unsaturation and head group charge, the type of proteins and receptors embedded that transduce unique signal pathways or fulfill enzymatic roles, and the number of cholesterol embedded, which directly affects the cells fluidity and surface tension²⁵.

The functionalization of nanoparticles affects how they will be internalized into the cell. Smaller nanoparticles (< 10 nm in diameter) can diffuse through and target most cells in the body while larger nanoparticles (> 500 nm in diameter) can only target cells that have advanced rearrangement machinery that can optimally rearrange their cytoskeleton to perform phagocytosis. Nanoparticle shape is another tunable property that affects its cellular uptake. Uptake for spherical nanoparticles is the highest, followed by cubical nanoparticles and then rods²⁶. Lastly, the nanoparticle's overall charge affects uptake and specificity. Nanoparticle charge can be easily functionalized and greatly influence how the nanoparticle will behave in the biological environment. In general, positively charged nanoparticles are internalized into the cell more efficiently compared to negatively charged nanoparticles, however, multiple studies show the opposite, and other studies suggest that charge density plays a large role in the biological fate of nanoparticles²⁷. Charge functionalization also can determine the targetability of nanoparticles, for example, positively charged LNPs are used in gene editing, as they target DNA easier due to their negatively charged phosphate backbone²⁸. Exploring these parameters further may yield further insight into nanoparticles' biological interactions.

Recent studies show that the formation of the protein corona around the surface of a nanoparticle can directly affect how that nanoparticle will interact with the plasma membrane⁴.

Motifs of various proteins adsorbed to the nanoparticle surface have the potential to be recognized by external cellular receptors as displayed in figure 1⁴. After recognition, the cellular receptors can induce signaling pathways that activate advanced internalization machinery in the cell²⁹. Further research is needed to understand how certain proteins in human serum can be targeted to adsorb to the nanoparticle surface, and how these protein motifs can be tailored to improve nanoparticle targetability⁴.

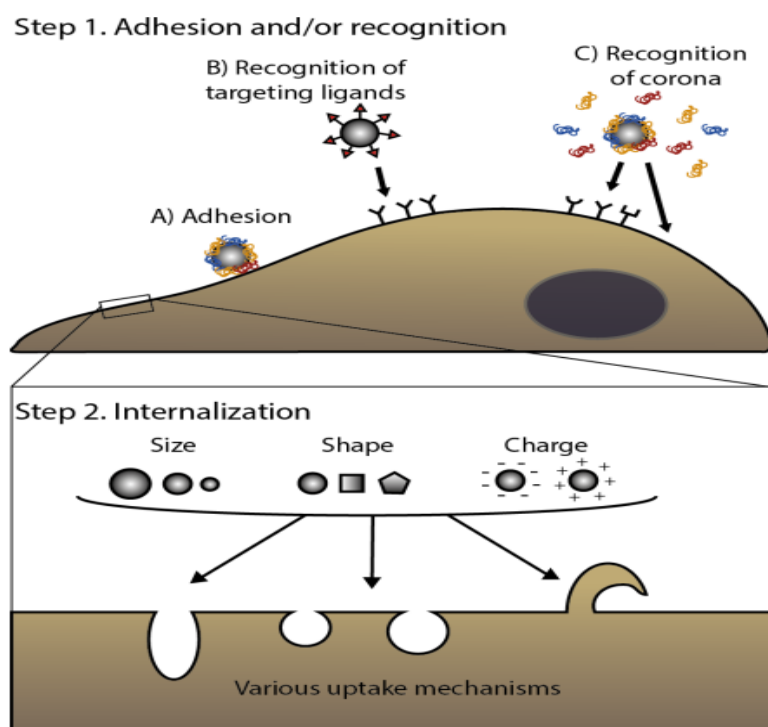


Figure 1: Step 1. The interaction of nano-sized materials at the cellular surface by adhesion to the membrane, b) recognition by cellular receptors through targeting ligands, or c) recognition by cellular receptors through protein motifs. Step 2. The various functionalization of nanoparticles affects cellular uptake. Image adapted from, “*Interactions at the cell membrane and pathways of internalization of nano-sized materials for nanomedicine*,” by Francia *et al.* 2020.

The cellular membrane behaves as a mechanobiological unit that encompasses many physical processes, such as surface pressure which directly relates to membrane tension. Membrane tension is heavily linked to cell migration and membrane trafficking, determining the adsorption and uptake of all molecules, including nanoparticles³⁰. Some studies found that

membrane tension directly affects the permeability of nanoparticles adsorbed to the cellular membrane surface³¹. How membrane tension affects the migration of materials across its surface is yet to be fully understood, and further experimentation may yield insight into how to engineer nanoparticles for medicinal purposes when faced with this parameter.

When it comes to nanoparticle adsorption, there are no quantitative measurements that explain the affinity of their binding to various cellular environments. Binding affinity is a common measurement to discern the toxicity of various objects to biological materials³². Quantifying the binding affinity of AuNPs in the biological environment may help us further understand what biological factors play the most significant role in AuNP uptake and further help the medical engineering for AuNPs in improving their targetability.

1.4: Aim of research

To this end, we hope to quantify and explain the binding affinity constant PEGylated gold nanoparticles have to various synthetic lipid membranes. It is known that the surface pressure and chemical nature of the phospholipid plays a part in the dispersion and uptake of nanoparticles³³. It is hypothesized that the phospholipid head group and nanoparticle's charge density play a significant role in affecting AuNP adsorption. Through utilizing uniquely charged phospholipid headgroups in tandem with charged capped AuNPs may we discern the efficacy of our experimental design in determining K_b and elucidate the effect of AuNP surface charge on their adsorption to the lipid membrane⁴. The AuNPs to be used in this study will be capped with thiol-PEG ligands terminated with an amine group.

The methodology to be used in this study includes the spreading of a single phospholipid solution onto an aqueous phase held in a petri dish and brought to saturation at this air/water interface, to form a single, monolayer. Measurements of monolayer surface pressure will be made using a Langmuir balance. PEGylated AuNPs are injected beneath the monolayer using a micro syringe. Injecting them into the subphase below the membrane is a representative means of AuNP exposure in the biological environment³³. A UV-Vis spectrometer will be used to measure the absorbance at the subphase over time, which represents the time it takes for the nanoparticles to adsorb to the lipid monolayer. This change in nanoparticle concentration in the subphase over time will be analyzed with Michaelis-Menten binding saturation kinetics and Langmuir Adsorption Isotherm Kinetics to quantify the binding constant of AuNP. Thus, this investigation will use this experimental methodology to be the first study to quantify the binding affinity of AuNPs to a monolayer environment and determine the role of lipid class and membrane surface pressure plays on AuNP adsorption.

Chapter 2

Materials & Methodology

2.1: Reagents and Solutions

Reagents used for these experiments were obtained from Sigma Aldrich (Oakville, ON, Canada) unless otherwise noted. Reagents used include chloroauric acid (HAuCl_4), hydroquinone ($\text{C}_6\text{H}_6\text{O}_2$), sodium citrate tribasic dihydride, thiol-polyethylene glycol-amine (7500Da, HS-PEG-NH₂), chloroform (CHCl_3). 1,2-dipalmitoyl-sn-glycerol-3-phosphocholine (DPPC) and 16:0-18:1 PG • 1-Hexadecanoyl-2-(9Z-Octadecenoyl)-sn-Glycero-3-Phosphoglycerol (POPG) were purchased from Avanti Polar Lipids (Birmingham, Al, USA). For comparison, the chemical structure of the two phospholipids used in this study are displayed in figure 2.

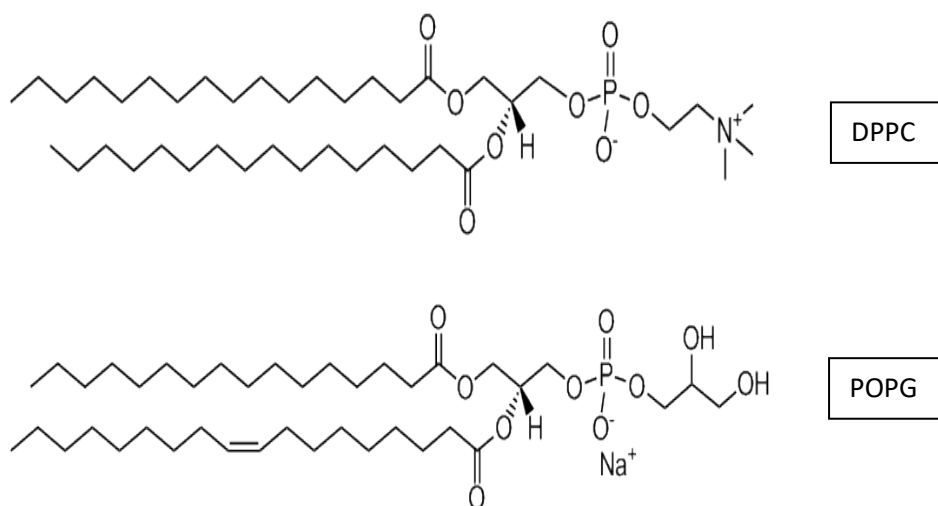


Figure 2: The chemical structure of DPPC and POPG, 2 of the lipids used in this study.

The difference in phospholipid structure allows us to determine the efficacy in our measurement of K_b through expecting different K_b values for each interaction.

2.2: Nanoparticle Synthesis and Characterization

The 75 nm diameter gold nanoparticles (AuNP) were synthesized following modifying procedures developed by Chou and Chen³⁴. Sodium tribasic citrate dihydrate (1% w/v), hydroquinone (3% w/v), and nanoparticle seed solutions were prepared fresh on the day of synthesis.

Nanoparticle seeds (15 nm) were first developed by adding 1% H₂AuCl₄ to deionized H₂O in an Erlenmeyer flask. The flask was rapidly stirred and heated until boiling was observed, at which point sodium tribasic citrate dihydrate was added to the solution. Once the solution developed a deep red color, the solution was placed in an ice bath to cool. Particle seed size was confirmed with a UV-Vis spectrometer.

The growth solution was prepared in a round bottom flask (rbf). Deionized H₂O, 1% H₂AuCl₄ and the particle seed solution prepared earlier were added to the flask and stirred at room temperature. 1% Sodium tribasic citrate dihydrate and 1% Hydroquinone were then added in quick succession to the flask which was left to stir for 10 minutes.

The concentration of AuNPs in the growth solution was determined utilizing a Varian UV-Vis spectrometer (Cat#500031) with tables and equations developed by Haiss *et al.* 2007³⁵. The concentration of nanoparticles was calculated using equation 1 and the extinction constant was gathered from Haiss *et al.* 2007. It is noteworthy to state this method is only applicable to AuNP between 5-100 nm in diameter.

Equation 1:
$$[\text{AuNP}] = A_{450}/\epsilon_{450}$$

The size of these AuNPs was determined using transmission electron microscopy (TEM). Images developed using TEM determined the actual size of our AuNPs was 73 ± 5 nm.

Once the size and concentration of the nanoparticles were determined, the total surface area of nanoparticles in solution was determined. The ratio of HS-PEG-NH₂ added to the nanoparticle solution was 5 PEG molecules per nm² of nanoparticle surface area in solution. This amount equated to 186 μmol of PEG being added to solution. The AuNP solution was heated to 60°C. Powdered HS-PEG-NH₂ was dissolved in deionized water and added to the solution which was left at that temperature for one hour. This allowed ligand exchange between citrate and the PEG molecules to occur. The nanoparticle solution was then washed with deionized water via centrifugation 3 times at 2000 rpm for 40 minutes.

Our AuNPs zeta potential was measured using a Dynamic Light Scattering Spectrometer (DLS). The zeta potential of our nanoparticles was determined to be -33 ± 1 mV. While unsuspected due to our PEG ligands having an amine terminus, it could be eluded that not enough time was taken to ensure complete ligand exchange between PEG and citrate.

2.3 Membrane Exposure

Deionized water was placed in a petri dish and heated to 30°C. The synthetic lipid membrane was spread at the air-water interface. The powdered lipid-containing POPG or DPPC was suspended in CHCl₃ to a final concentration of 0.1 mM and administered to the interface dropwise utilizing a micro-glass syringe until the monolayer reached a surface pressure of 30 mN/m that was measured using a Langmuir trough.

The method of nanoparticle exposure is a modified procedure published in MacCormack et al. 2017. The AuNP solution is injected into the subphase, below the lipid monolayer using a glass syringe. The subphase was mixed slowly, utilizing a stir bar. The initial concentration of nanoparticles injected into the subphase was varied at 1.89×10^{-3} nM, 2.56×10^{-3} nM 3.78×10^{-3} nM, 5.68×10^{-3} nM, 6.56×10^{-3} nM and 7.57×10^{-3} nM, chosen so absorbance measurements would be in the UV-Vis detection range.

2.4 Michaelis-Menten Calculations

Aliquots in 50 μ L volumes of the subphase were gathered every 5 seconds using a glass, micro syringe. Aliquots were placed into a micro-glass cuvette and their absorbance was measured using a UV-Vis spectrometer. The concentration of AuNP in the subphase was calculated using equation 1. The concentration of AuNP adsorbed to the monolayer surface was determined from the decrease in the concentration of AuNP in the subphase over time. This was plotted as moles of AuNP adsorbed to the lipid monolayer over time. The rate of AuNP adsorption over time (v_0) was determined from the slope of the plot. This procedure was repeated in triplicate and averaged, including the confidence interval at 95%. Using v_0 , we developed a Michaelis–Menten binding kinetics saturation curve, where the initial concentration of AuNP in the subphase was plotted against V_0 .

A binding saturation curve based on Michaelis–Menten kinetics was used to determine the dissociation constant of AuNP binding to the lipid monolayer. The program, Prism by GraphPad, version 9, was used to calculate the dissociation constant (k_D) and max binding concentration (B_{\max}) from our data through a nonlinear curve fit explained in equation 2.

Equation 2:
$$v_0 = \frac{B_{max} \times [AuNP]}{k_D + [AuNP]}$$

The binding affinity (K_b) is the inverse of k_D and was determined using equation 3.

Equation 3:
$$K_b = \frac{1}{\kappa_D}$$

2.6: Langmuir Adsorption Isotherm

The Langmuir adsorption isotherm was another model employed to determine K_b . The data we collected earlier was used in tandem with the linear form of equation 4 (shown in equation 5), where θ is defined as the coverage density.

Equation 4:
$$\theta = \frac{K_b[AuNP]}{1 + K_b[AuNP]}$$

θ was determined as the total surface area of nanoparticles adsorbed to the monolayer divided by the total surface area available in the lipid monolayer. Transforming this fit to a linear regression allowed us to determine K_b from the slope of the regression. The equation for the linear regression is explained by equation 5.

Equation 5:
$$\frac{1}{\theta} = \frac{1}{K_b[AuNP]} + 1$$

Chapter 3

Results

3.1: The binding affinity of gold nanoparticles determined using Michaelis Menten

To investigate a few driving forces of nanoparticle to cellular membrane adsorption, the binding affinity constant of 75 nm gold nanospheres (AuNP) functionalized with NH₂ terminated 7.5 kDa PEG ligand to an artificial lipid monolayer was quantified first utilizing Michaelis-Menten kinetics. To begin, a phospholipid monolayer of DPPC (0.1mM) was spread across a petri dish until brought to saturation where it exhibited a surface tension of 30 mN/m when measured with a Langmuir balance Wilhelmy plate apparatus. Aqueous AuNP was injected below the surface at the bottom of the Petrie dish at volumes to induce initial AuNP concentrations of 1.89×10^{-3} nM, 2.56×10^{-3} nM, 3.78×10^{-3} nM, 5.68×10^{-3} nM, 6.56×10^{-3} nM, and 7.57×10^{-3} nM. Immediately after injection, a portion of the AuNP solution was observed to rise to the surface where the lipid monolayer was present. The AuNP concentration in the solution decreased rapidly over time. Within the first minute, the maximum binding was achieved, with no change in nanoparticle concentration in the subphase, indicated by UV-Vis measurements. The binding saturation curves produced for AuNP adsorption to DPPC and POPG at 30°C produced using Prism fit to equation 2 can be observed in Figure 3 and the values K_D , K_b , and B_{max} calculated using Prism are displayed in table 1. The calculated K_b from the binding saturation analysis indicates that DPPC has a greater affinity for the binding of these AuNPs compared to POPG.

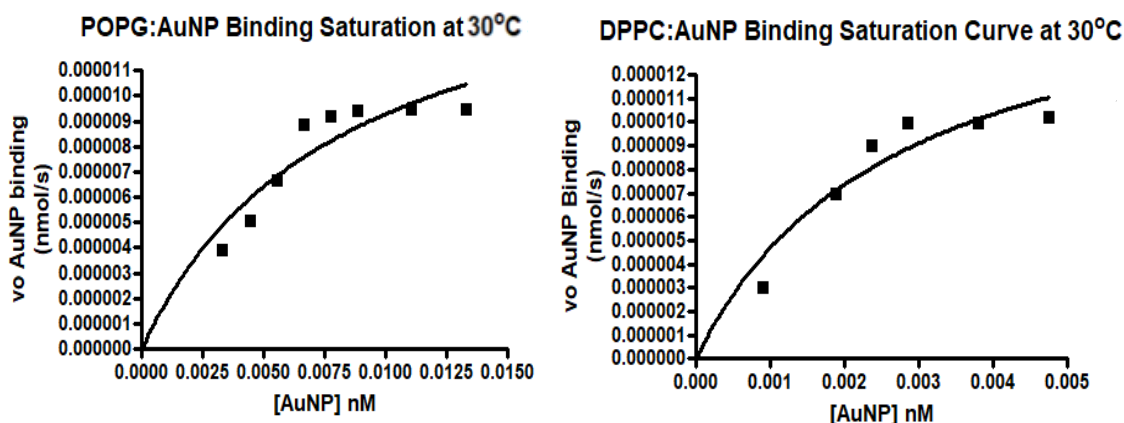


Figure 3: The comparison of binding saturation curves for AuNPs to the surface of a DPPC monolayer and a POPG monolayer at 30°C. Curves were developed through UV-Vis analysis and the Prism program, which fitted equation 2 to determine data. Data is represented as a nonlinear curve of nmol AuNP adsorbed per second (nmol/s) over the initial AuNP concentration [AuNP]

Table 1: The table of constants (k_D , B_{max} , K_b), produced using Michaelis–Menten Binding Kinetics through Prism determined through best fit data from equation 2.

	DPPC	POPG
B_{max} (nmol/s)	$2.53 \times 10^{-6} \pm 1.61 \times 10^{-6}$	$2.87 \times 10^{-5} \pm 1.88 \times 10^{-6}$
k_D (nM)	$2.87 \times 10^{-3} \pm 2.53 \times 10^{-3}$	$3.70 \times 10^{-3} \pm 2.42 \times 10^{-3}$
K_b	348 ± 284	270 ± 160

The distribution range of the K_b values shows that while we were able to determine a K_b value, the Michaelis–Menten Binding Saturation Kinetics was not as precise as we would have hoped. Furthermore, this model is best used for describing enzyme-substrate interactions which are not a representative of the binding saturation experience by our AuNPs to a lipid monolayer.

3.2: The binding affinity of gold nanoparticles determined using Langmuir Adsorption Isotherm

We wanted to test the Langmuir adsorption isotherm to see if we could develop K_b from the concentration data we developed earlier. This model also felt more representative of our experimental system, where similar to a surface binding a molecule is determined by its coverage density, AuNPs from the subphase that are adsorbing to the surface of the monolayer is determined by the total surface area on the phospholipid monolayer available for the AuNP to adsorb to. The Langmuir adsorption isotherm was developed for AuNP adsorption to DPPC and POPG monolayers using equation 4 and transformed to a linear regression using equation 5. These graphs can be observed in Figure 4. The K_b values were determined from the slope of the linear regression and their values are displayed in table 2. The calculated K_b from the Langmuir adsorption isotherm also indicates that DPPC has a greater affinity for the binding of these AuNPs compared to POPG.

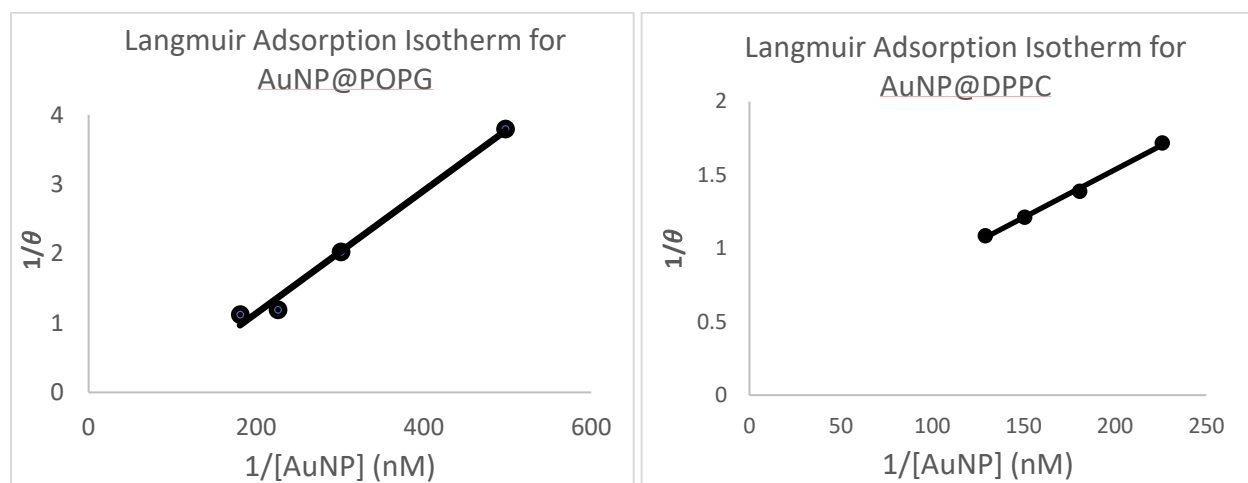


Figure 4: The comparison of binding saturation curves for AuNPs to the surface of a DPPC monolayer and a POPG monolayer at 30°C. Curves were developed through UV-Vis analysis and fitted to a linear regression using equations 4 and 5. Data is represented as a linear regression of $1/\theta$ coverage density (θ) over the initial $1/[AuNP]$. $R^2 = 0.99$ for both regressions.

Table 2: The determined K_b values determined using the Langmuir Adsorption isotherm and equations 4 and 5.

	DPPC	POPG
K_b	213 ± 6	115 ± 8

The Langmuir Adsorption Isotherm model developed a more sensitive and precise range of K_b for AuNP adsorption to DPPC and POPG. The significance of the difference between the two determined K_b values was evaluated using a two-tailed paired t-test and a 95 % confidence interval. The resulting p-value was 0.003168 ($p > 0.05$), which indicated that the binding affinity constant for AuNP@DPPC is significantly larger than AuNP@POPG.

Chapter 4

Discussion & Conclusions

4.1: Model and Experimental Evaluation

The purpose of this project was to determine an effective method suitable for determining the binding affinity constant of AuNP adsorption to synthetic phospholipid monolayers. The assumption for this system is that AuNPs will bind to the phospholipid monolayer and not penetrate through the monolayer. The AuNPs used in this study have displayed affinity toward the surface of the lipid monolayers. Alluded to by the UV-Vis measurements, the disappearance from AuNP in the subphase indicates adsorption of AuNPs to the lipid monolayer have occurred. Physical observations of the AuNPs once injected into the subphase also confirm this notion, where portions of AuNP solution was seen to rise rapidly from the bottom of the petri dish where it was injected to the top where the monolayer was.

The two models used in the comparison were the Michaelis-Menten Binding Saturation Kinetics and the Langmuir Adsorption Isotherm. K_b was determined using both models, however, the Langmuir adsorption isotherm developed a more sensitive and precise range. The Michaelis-Menten model is traditionally used to describe enzyme and substrate interactions, where usually an enzyme will have a single active site that binds the substrate of interest. Furthermore, a biochemical reaction is expected, where the substrate is transformed into a product and then released³⁶. This means the B_{max} value, which is the maximum rate of binding, is limited by the biochemical reaction of the substrate to product holds no meaning for our experimental system³⁷.

In our experimental system, we are expecting the AuNPs to adsorb to the surface of the monolayer, however, no biochemical reaction is expected. Rather, AuNPs will continue to bind to the surface of the monolayer until the monolayer is completely covered. Thus, a Langmuir adsorption isotherm seems to be more representative of this assumption, whereas similarly, a Langmuir adsorption isotherm is a model developed to describe the equilibrium between adsorbate and adsorbent, in which adsorption is limited by the coverage density of the adsorbant³⁸. There is no assumption of a chemical or biochemical reaction, only the adsorption of one object to another.

Our data range was limited by the detection range of the UV-Vis spectrometer, the smallest possible concentration of AuNP in a solution that could be measured being 1.89×10^{-3} nM. Thus, the lowest coverage density we could determine was 0.33. Potentially other methods beyond UV-Vis, if available to the lab will be able to measure nanoparticle concentrations below this range and develop the full regression data set for this AuNP interaction. Any coverage density measurement below 1 is valuable in determining K_b through the linear regression analysis³⁹.

4.2: Biological Relevance of K_b

In comparing the binding kinetics of AuNP to the surface of DPPC and POPG, we could also understand the driving forces that influence nanoparticle adsorption to a system resembling a cellular surface. K_b values indicate that there was a significantly higher degree of binding affinity ($p < 0.05$) for our AuNPs to DPPC over POPG. There is a couple of reasons as to why this might be. First, DPPC has a zwitterionic head group and POPG has an anionic head group,

meaning charge interactions play a role in nanoparticle adsorption. Zeta potential of our AuNPs indicated a net negative charge on the surface of our nanoparticles, meaning that because DPPC has a positive charge in its headgroup, and that portion of the headgroup is the most exposed to the subphase, the charge difference between our AuNPs and the DPPC head group lead to a greater binding affinity. The second reason why there was a greater affinity of our AuNP for the DPPC monolayer may be due to the single unsaturation that POPG has in its fatty acid chain. This would cause individual POPG molecules to be more spread out from one another in the monolayer, while DPPC molecules can be more packed, meaning more headgroups are available to drive AuNP adsorption⁴⁰.

It is important to take into consideration the nature of DPPC in this experiment. While the headgroup is zwitterionic, the pressure of the monolayer plays a huge role in the chemical nature of DPPC at the subphase. Some experiments show that DPPC head group tilt (altered by surface pressure) can determine whether both charges, the phosphate and ammonia portions of the head are present at the interface or whether only the ammonia portion of the head group is at the interface⁴¹. This would greatly affect the binding affinity constant for AuNP adsorption to DPPC, where K_b should be highest for our AuNP design when DPPC is oriented with only its ammonia portion of the headgroup at the interface³³. Our DPPC monolayer surface pressure was measured at 30 mN/m. According to previous literature, this high pressure should tilt the headgroup, with ammonia being closer to the interface and the phosphate portion of the headgroup being pushed back. The tilt angle between these two functional groups of DPPC at 30°C and an air/water interface is 40 ± 5 ⁴². This means our phospholipid environment at the interface primarily expressed a net positive charge. This would've further driven the binding affinity for our nanoparticles to the DPPC monolayer.

4.3: Future Directions

While we were able to develop a methodology to determine K_b for AuNP adsorption, our monolayer system is not entirely representative of a common cellular membrane found in biological organisms. We would want to understand the relevance of our K_b measurements for AuNP interactions to a phospholipid monolayer compared to a complex cellular system. This may be experimentally conducted with pre-developed cell cultures or in a synthetic system. Furthermore, utilizing a synthetic cellular membrane would further let us understand the individual effects each component brings to K_b such as cholesterol, glycoproteins, glycolipids, and other phospholipid compositions.

Proteins in biological serum often spontaneously adsorb to the surface of nanoparticles, forming a biomolecular corona²⁹. This process is ubiquitous for AuNPs. Thus, we believe it to be very important to understand how the protein corona composition affects nanoparticle adsorption to the cellular membrane.

4.4: Conclusion

This project developed an experimental method for determining the binding affinity constant of AuNPs to the surface of phospholipids monolayer. Of the two models tested the Langmuir Adsorption Isotherm gave a more sensitive and precise range for K_b . This model also better represented our experimental method. The developed K_b values for our two separate phospholipid monolayers elucidated that charge interactions between the lipid head group and AuNP surface potential play a significant role in determining the strength of adsorption.

References

- (1) Kim, B. Y. S.; Rutka, J. T.; Chan, W. C. W. Nanomedicine. *N Engl J Med* **2010**, *363* (25), 2434–2443. <https://doi.org/10.1056/NEJMra0912273>.
- (2) Sindhvani, S.; Chan, W. C. W. Nanotechnology for Modern Medicine: Next Step towards Clinical Translation. *J Intern Med* **2021**. <https://doi.org/10.1111/joim.13254>.
- (3) Chou, L. Y. T.; Ming, K.; Chan, W. C. W. Strategies for the Intracellular Delivery of Nanoparticles. *Chem. Soc. Rev.* **2010**, *40* (1), 233–245. <https://doi.org/10.1039/C0CS00003E>.
- (4) Francia, V.; Yang, K.; Deville, S.; Reker-Smit, C.; Nelissen, I.; Salvati, A. Corona Composition Can Affect the Mechanisms Cells Use to Internalize Nanoparticles. *ACS Nano* **2019**, *13* (10), 11107–11121. <https://doi.org/10.1021/acsnano.9b03824>.
- (5) Gulati, S.; Sachdeva, M.; Bhasin, K. K. Capping Agents in Nanoparticle Synthesis: Surfactant and Solvent System. *AIP Conference Proceedings* **2018**, *1953* (1), 030214. <https://doi.org/10.1063/1.5032549>.
- (6) Javed, R.; Zia, M.; Naz, S.; Aisida, S.; Ul Ain, N.; Ao, Q. Role of Capping Agents in the Application of Nanoparticles in Biomedicine and Environmental Remediation: Recent Trends and Future Prospects. *Journal of Nanobiotechnology* **2020**, *18*, 172. <https://doi.org/10.1186/s12951-020-00704-4>.
- (7) Plowman, B. J.; Compton, R. G. Inhibition of Cu Underpotential Deposition on Au Nanoparticles: The Role of the Citrate Capping Agent and Nanoparticle Size. *ChemElectroChem* **2014**, *1* (6), 1009–1012. <https://doi.org/10.1002/celec.201400015>.
- (8) Mohapatra, A.; Uthaman, S.; Park, I.-K. Chapter 10 - Polyethylene Glycol Nanoparticles as Promising Tools for Anticancer Therapeutics. In *Polymeric Nanoparticles as a Promising Tool for Anti-cancer Therapeutics*; Kesharwani, P., Paknikar, K. M., Gajbhiye, V., Eds.; Academic Press, 2019; pp 205–231. <https://doi.org/10.1016/B978-0-12-816963-6.00010-8>.
- (9) Schöttler, S.; Becker, G.; Winzen, S.; Steinbach, T.; Mohr, K.; Landfester, K.; Mailänder, V.; Wurm, F. R. Protein Adsorption Is Required for Stealth Effect of Poly(Ethylene Glycol)- and Poly(Phosphoester)-Coated Nanocarriers. *Nat Nanotechnol* **2016**, *11* (4), 372–377. <https://doi.org/10.1038/nnano.2015.330>.
- (10) Florindo, H. F.; Kleiner, R.; Vaskovich-Koubi, D.; Acúrcio, R. C.; Carreira, B.; Yeini, E.; Tiram, G.; Liubomirski, Y.; Satchi-Fainaro, R. Immune-Mediated Approaches against COVID-19. *Nature Nanotechnology* **2020**, *15* (8), 630–645. <https://doi.org/10.1038/s41565-020-0732-3>.
- (11) Kozma, G. T.; Mészáros, T.; Vashegyi, I.; Fülöp, T.; Örfi, E.; Dézsi, L.; Rosivall, L.; Bavli, Y.; Urbanics, R.; Mollnes, T. E.; Barenholz, Y.; Szebeni, J. Pseudo-Anaphylaxis to Polyethylene Glycol (PEG)-Coated Liposomes: Roles of Anti-PEG IgM and Complement Activation in a Porcine Model of Human Infusion Reactions. *ACS Nano* **2019**, *13* (8), 9315–9324. <https://doi.org/10.1021/acsnano.9b03942>.
- (12) Wylon, K.; Dölle, S.; Worm, M. Polyethylene Glycol as a Cause of Anaphylaxis. *Allergy, Asthma & Clinical Immunology* **2016**, *12* (1), 67. <https://doi.org/10.1186/s13223-016-0172-7>.
- (13) Nakamura, T.; Kawai, M.; Sato, Y.; Maeki, M.; Tokeshi, M.; Harashima, H. The Effect of Size and Charge of Lipid Nanoparticles Prepared by Microfluidic Mixing on Their Lymph

- Node Transitivity and Distribution. *Mol. Pharmaceutics* **2020**, *17* (3), 944–953. <https://doi.org/10.1021/acs.molpharmaceut.9b01182>.
- (14) Brandelli, A. The Interaction of Nanostructured Antimicrobials with Biological Systems: Cellular Uptake, Trafficking and Potential Toxicity. *Food Science and Human Wellness* **2020**, *9* (1), 8–20. <https://doi.org/10.1016/j.fshw.2019.12.003>.
- (15) Vishwakarma, V.; Samal, S. S.; Manoharan, N. Safety and Risk Associated with Nanoparticles - A Review. *Journal of Minerals and Materials Characterization and Engineering* **2010**, *9* (5), 455–459. <https://doi.org/10.4236/jmmce.2010.95031>.
- (16) Mostafalou, S.; Mohammadi, H.; Ramazani, A.; Abdollahi, M. Different Biokinetics of Nanomedicines Linking to Their Toxicity; an Overview. *Daru* **2013**, *21* (1), 14. <https://doi.org/10.1186/2008-2231-21-14>.
- (17) Kessler, R. Engineered Nanoparticles in Consumer Products: Understanding a New Ingredient. *Environ Health Perspect* **2011**, *119* (3), A120–A125.
- (18) Kirchner, C.; Javier, A. M.; Susha, A. S.; Rogach, A. L.; Kreft, O.; Sukhorukov, G. B.; Parak, W. J. Cytotoxicity of Nanoparticle-Loaded Polymer Capsules. *Talanta* **2005**, *67* (3), 486–491. <https://doi.org/10.1016/j.talanta.2005.06.042>.
- (19) Lee, S. H.; Bae, K. H.; Kim, S. H.; Lee, K. R.; Park, T. G. Amine-Functionalized Gold Nanoparticles as Non-Cytotoxic and Efficient Intracellular siRNA Delivery Carriers. *International Journal of Pharmaceutics* **2008**, *364* (1), 94–101. <https://doi.org/10.1016/j.ijpharm.2008.07.027>.
- (20) Huang, Y.-W.; Cambre, M.; Lee, H.-J. The Toxicity of Nanoparticles Depends on Multiple Molecular and Physicochemical Mechanisms. *Int J Mol Sci* **2017**, *18* (12), 2702. <https://doi.org/10.3390/ijms18122702>.
- (21) Kong, F.-Y.; Zhang, J.-W.; Li, R.-F.; Wang, Z.-X.; Wang, W.-J.; Wang, W. Unique Roles of Gold Nanoparticles in Drug Delivery, Targeting and Imaging Applications. *Molecules* **2017**, *22* (9), 1445. <https://doi.org/10.3390/molecules22091445>.
- (22) Vines, J. B.; Yoon, J.-H.; Ryu, N.-E.; Lim, D.-J.; Park, H. Gold Nanoparticles for Photothermal Cancer Therapy. *Frontiers in Chemistry* **2019**, *7*, 167. <https://doi.org/10.3389/fchem.2019.00167>.
- (23) Tavares, A. J.; Poon, W.; Zhang, Y.-N.; Dai, Q.; Besla, R.; Ding, D.; Ouyang, B.; Li, A.; Chen, J.; Zheng, G.; Robbins, C.; Chan, W. C. W. Effect of Removing Kupffer Cells on Nanoparticle Tumor Delivery. *PNAS* **2017**, *114* (51), E10871–E10880. <https://doi.org/10.1073/pnas.1713390114>.
- (24) Shaw, A. W.; Pureza, V. S.; Sligar, S. G.; Morrissey, J. H. The Local Phospholipid Environment Modulates the Activation of Blood Clotting. *J Biol Chem* **2007**, *282* (9), 6556–6563. <https://doi.org/10.1074/jbc.M607973200>.
- (25) Cooper, G. M. Structure of the Plasma Membrane. *The Cell: A Molecular Approach. 2nd edition* **2000**.
- (26) Carnovale, C.; Bryant, G.; Shukla, R.; Bansal, V. Size, Shape and Surface Chemistry of Nano-Gold Dictate Its Cellular Interactions, Uptake and Toxicity. **2016**. <https://doi.org/10.1016/J.PMATSCI.2016.04.003>.
- (27) Xiao, K.; Li, Y.; Luo, J.; Lee, J. S.; Xiao, W.; Gonik, A. M.; Agarwal, R. G.; Lam, K. S. The Effect of Surface Charge on in Vivo Biodistribution of PEG-Oligocholic Acid Based Micellar Nanoparticles. *Biomaterials* **2011**, *32* (13), 3435–3446. <https://doi.org/10.1016/j.biomaterials.2011.01.021>.

- (28) Xiao, Y.; Shi, K.; Qu, Y.; Chu, B.; Qian, Z. Engineering Nanoparticles for Targeted Delivery of Nucleic Acid Therapeutics in Tumor. *Molecular Therapy - Methods & Clinical Development* **2019**, *12*, 1–18. <https://doi.org/10.1016/j.omtm.2018.09.002>.
- (29) Francia, V.; Schiffelers, R. M.; Cullis, P. R.; Witzigmann, D. The Biomolecular Corona of Lipid Nanoparticles for Gene Therapy. *Bioconjugate Chem.* **2020**, *31* (9), 2046–2059. <https://doi.org/10.1021/acs.bioconjchem.0c00366>.
- (30) Sitarska, E.; Diz-Muñoz, A. Pay Attention to Membrane Tension: Mechanobiology of the Cell Surface. *Curr Opin Cell Biol* **2020**, *66*, 11–18. <https://doi.org/10.1016/j.ceb.2020.04.001>.
- (31) Lin, J.; Zhang, H.; Chen, Z.; Zheng, Y. Penetration of Lipid Membranes by Gold Nanoparticles: Insights into Cellular Uptake, Cytotoxicity, and Their Relationship. *ACS Nano* **2010**, *4* (9), 5421–5429. <https://doi.org/10.1021/nn1010792>.
- (32) Smaoui, M. R.; Orland, H.; Waldspühl, J. Probing the Binding Affinity of Amyloids to Reduce Toxicity of Oligomers in Diabetes. *Bioinformatics* **2015**, *31* (14), 2294–2302. <https://doi.org/10.1093/bioinformatics/btv143>.
- (33) Malek, M.; Curtis, I. S.; MacCormack, T. J.; Meli, M.-V. Charged and Neutral Au Nanoparticles Interact Differently with Langmuir Film-Based Synthetic Membranes: Implications for Nanoparticle Uptake and Membrane Protein Activity. *ACS Appl. Nano Mater.* **2020**, *3* (9), 9276–9284. <https://doi.org/10.1021/acsnm.0c01906>.
- (34) Chou, L. Y. T.; Chan, W. C. W. Fluorescence-Tagged Gold Nanoparticles for Rapidly Characterizing the Size-Dependent Biodistribution in Tumor Models. *Adv Healthc Mater* **2012**, *1* (6), 714–721. <https://doi.org/10.1002/adhm.201200084>.
- (35) Haiss, W.; Thanh, N. T. K.; Aveyard, J.; Fernig, D. G. Determination of Size and Concentration of Gold Nanoparticles from UV-Vis Spectra. *Anal Chem* **2007**, *79* (11), 4215–4221. <https://doi.org/10.1021/ac0702084>.
- (36) Jun, H.; Rong, Y.; Yih, C.; Ho, J.; Cheng, W.; Kiang, T. K. L. Comparisons of Four Protein-Binding Models Characterizing the Pharmacokinetics of Unbound Phenytoin in Adult Patients Using Non-Linear Mixed-Effects Modeling. *Drugs R D* **2020**, *20* (4), 343–358. <https://doi.org/10.1007/s40268-020-00323-2>.
- (37) Raaijmakers, J. G. W. Statistical Analysis of the Michaelis-Menten Equation. *Biometrics* **1987**, *43* (4), 793–803. <https://doi.org/10.2307/2531533>.
- (38) Yang, T.-H.; Shi, Y.; Janssen, A.; Xia, Y. Surface Capping Agents and Their Roles in Shape-Controlled Synthesis of Colloidal Metal Nanocrystals. *Angew Chem Int Ed Engl* **2020**, *59* (36), 15378–15401. <https://doi.org/10.1002/anie.201911135>.
- (39) Subramanyam, B.; Das, A. Linearised and Non-Linearised Isotherm Models Optimization Analysis by Error Functions and Statistical Means. *J Environ Health Sci Eng* **2014**, *12*, 92. <https://doi.org/10.1186/2052-336X-12-92>.
- (40) Chen, K. L.; Bothun, G. D. Nanoparticles Meet Cell Membranes: Probing Nonspecific Interactions Using Model Membranes. *Environ. Sci. Technol.* **2014**, *48* (2), 873–880. <https://doi.org/10.1021/es403864v>.
- (41) Shen, H.; Wu, Z.; Zou, X. Interfacial Water Structure at Zwitterionic Membrane/Water Interface: The Importance of Interactions between Water and Lipid Carbonyl Groups. *ACS Omega* **2020**, *5* (29), 18080–18090. <https://doi.org/10.1021/acsomega.0c01633>.
- (42) Aikawa, T.; Okura, H.; Kondo, T.; Yuasa, M. Comparison of Carboxybetaine with Sulfobetaine as Lipid Headgroup Involved in Intermolecular Interaction between Lipids in

the Membrane. *ACS Omega* **2017**, 2, 5803–5812.
<https://doi.org/10.1021/acsomega.7b00574>.

Appendix

Supplemental Data

The standard AuNP characterization with UV-Vis

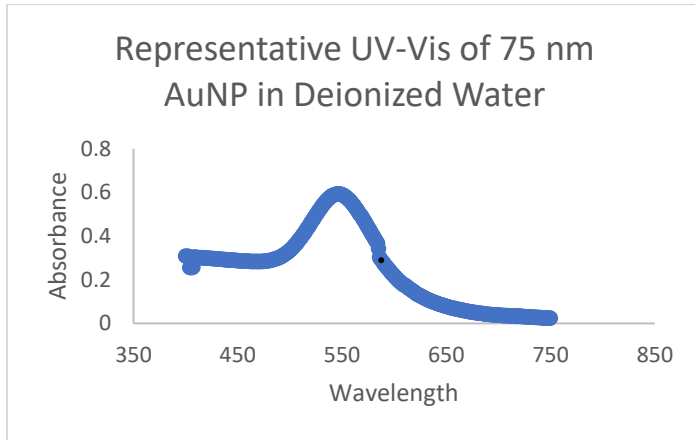


Figure A: A common UV-Vis run used to determine AuNP concentration.

TEM Images:

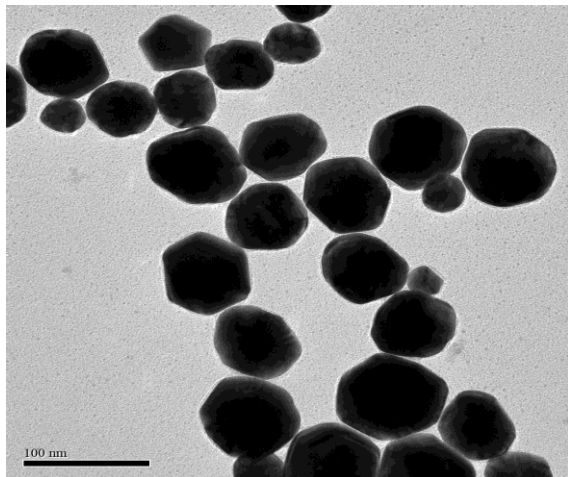


Figure B: TEM imaged of synthesized AuNPs utilizing the hydroquinone/citrate reduction developed by Chou et al. 2014